

Asymmetry Effects in Polarized Hadron Scattering

Yaw-Hwang Chen, Su-Long Nyeo¹

and

Chung-Yi Wu

Department of Physics, National Cheng Kung University,
Tainan, Taiwan 701, R.O.C

Abstract

We calculate the single-spin and double-spin asymmetry differential cross sections for the polarized hadron scattering $PP \rightarrow l^+l^- + jet$ up to $O(\alpha_s)$ by the helicity amplitude method. Numerical results of the differential cross sections, which can be used to probe the spin contents of the proton, are obtained from several sets of polarized parton distribution functions.

PACS:13.88.+e, 12.38.Bx, 12.38.QK

¹Author to whom all correspondence should be addressed.
E-mail: t14269@MAIL.NCKU.EDU.TW.

I. Introduction

In recent years, the determination of the spin contents of the nucleon has been the subject of a large number of work, which was initiated by the EMC experimental results [1] that the spin of the proton does not arise from its constituent quarks as expected in the naïve quark model; the valence quarks contribute very little to the spin of the nucleon.

Presently, there are three possibilities for explaining the EMC and other subsequent experimental results [2,3,4], namely (i) large sea quark polarization [5]; (ii) large gluon polarization [6]; and (iii) mediately large sea and gluon polarizations [7]. Since a different explanation leads to a different set of polarized parton distribution functions, the determination of the polarized parton densities by other experiments like polarized hadron-hadron scattering is very important for understanding of the spin contents of the nucleon. From the experiments, we can study the single-spin and double-spin asymmetries. For both initial protons longitudinally polarized, we study the double-spin asymmetries. Here the inclusive cross sections for the incoming hadrons' longitudinal polarizations are either parallel or antiparallel. From the experimental point of view, it is simpler to consider the single-spin asymmetries, where one of the initial hadron beams is longitudinally polarized and has positive or negative helicity. A nonzero single-spin asymmetry implies that some of the parton-parton scatterings involve parity-violating

weak interactions. Therefore, the single-spin asymmetries can also be used to probe parity-violating parton-parton subprocesses [8].

In this paper, we shall study the polarized $PP \rightarrow l^+l^- + jet$ scattering by the helicity amplitude method [9]. Both the single-spin and double-spin asymmetries are studied. At high energies, it is expected that virtual photon and virtual Z boson equally make important contributions to the lepton pair production. We organize the paper as follows. In section II, we shall use the helicity amplitude method to calculate the helicity amplitudes for the differential cross sections for the polarized hadron scattering. In section III, we calculate numerically the single and double asymmetries for the scattering. Finally, our conclusion is given in section IV.

II. Calculation of the Helicity Amplitudes

In this section, we shall calculate the amplitudes for the single-spin and double-spin asymmetry differential cross sections for the polarized $PP \rightarrow l^+l^- + jet$ scattering up to $O(\alpha_s)$ by the helicity amplitude method. We need to consider the following two parton subprocesses and their charge conjugates contributing to the dilepton production

$$G + q \rightarrow l^+l^- + q, \quad (1)$$

$$q + \bar{q} \rightarrow l^+l^- + G. \quad (2)$$

We denote $M(\lambda_1, \lambda_2; \lambda_3, \lambda_4, \lambda_5)$ as the helicity amplitude, where λ_1 and λ_2 are the helicities of the initial partons, while λ_3 , λ_4 and λ_5 are the helicities of the lepton pair l^+ , l^- , and the final parton, respectively. The nonvanishing tree-level amplitudes read

$$M(\lambda_1, \lambda_2; \lambda_3, \lambda_4, \lambda_5) = \begin{cases} M(\lambda_1, \lambda_2; \lambda_3, -\lambda_3, \lambda_2), & \text{for } G + q \rightarrow l^+l^- + q, \\ M(\lambda_1, -\lambda_1; \lambda_3, -\lambda_3, \lambda_5), & \text{for } q + \bar{q} \rightarrow l^+l^- + G. \end{cases}$$

The helicity amplitudes for figures 1.(a) and 1.(b) are $M(\lambda_1, \lambda_2; \lambda_3, -\lambda_3, \lambda_2)$, whereas those for figures 1.(c) and 1.(d) are $M(\lambda_1, -\lambda_1; \lambda_2, -\lambda_2, \lambda_3)$.

To evaluate the amplitudes, we first define some useful formulae and our convention. We denote the positive and negative helicity states by $|A_\pm\rangle$, which have the following properties:

$$\begin{aligned} (1 \pm \gamma_5) |A_\mp\rangle &= 0, \\ |A_+\rangle^c &= |A_-\rangle, \\ \langle A_\mp | B_\pm \rangle &= -\langle B_\mp | A_\pm \rangle, \\ \langle A_+ | \gamma_\mu | B_+ \rangle &= \langle B_- | \gamma_\mu | A_- \rangle, \end{aligned} \tag{3}$$

and, by Fierz rearrangement theorem,

$$\begin{aligned} \langle A_+ | \gamma_\mu | B_+ \rangle \langle C_- | \gamma^\mu | D_- \rangle &= 2\langle A_+ | D_- \rangle \langle C_- | B_+ \rangle, \\ \langle A_- | B_+ \rangle \langle C_- | D_+ \rangle &= \langle A_- | D_+ \rangle \langle C_- | B_+ \rangle + \langle A_- | C_+ \rangle \langle B_- | D_+ \rangle. \end{aligned} \tag{4}$$

The massless spinors with momentum p and helicity $\lambda = \pm$ are $u_{\pm}(p)$, $v_{\pm}(p)$, $\bar{u}_{\pm}(p)$ and $\bar{v}_{\pm}(p)$, which satisfy

$$\begin{aligned} \not{p}u(p) &= \not{p}v(p) = \bar{u}(p)\not{p} = \bar{v}(p)\not{p}, p^2 = 0, \\ (1 \pm \gamma_5)v_{\pm} &= (1 \mp \gamma_5)u_{\pm} = \bar{u}_{\pm}(1 \pm \gamma_5) = \bar{v}_{\pm}(1 \mp \gamma_5) = 0, \quad (5) \\ \bar{u}_{\pm}(p)\gamma_{\mu}u_{\pm}(p) &= \bar{v}_{\pm}(p)\gamma_{\mu}v_{\pm}(p) = 2p_{\mu}. \end{aligned}$$

For massless momentum p , we can write $\not{p} = |p_{+}\rangle\langle p_{+}| + |p_{-}\rangle\langle p_{-}|$ and use the convention

$$\begin{aligned} u_{\pm}(p) &= v_{\mp}(p) = |p_{\pm}\rangle, \\ \bar{u}_{\pm}(p) &= \bar{v}_{\mp}(p) = \langle p_{\pm}|, \quad (6) \\ |p_{\mp}\rangle &= |p_{\pm}\rangle^c. \end{aligned}$$

For simplicity, we shall write

$$\begin{aligned} \langle p_{-} | q_{+} \rangle &= \langle pq \rangle = -\langle qp \rangle, \\ \langle q_{+} | p_{-} \rangle &= \langle pq \rangle^* = -\langle qp \rangle^*, \quad (7) \\ |\langle pq \rangle|^2 &= 2p \cdot q. \end{aligned}$$

Finally, the gluon helicities are chosen to be

$$\not{\epsilon}_1^{\pm} = \frac{\pm\sqrt{2}}{\langle p_5^{\mp} | p_1^{\pm} \rangle} [|p_1^{\mp}\rangle\langle p_5^{\mp}| + |p_5^{\pm}\rangle\langle p_1^{\pm}|] \quad \text{for } G + q \rightarrow l^+l^- + q, \quad (8)$$

$$\not{\epsilon}_5^{\pm} = \frac{\pm\sqrt{2}}{\langle p_1^{\mp} | p_5^{\pm} \rangle} [|p_5^{\mp}\rangle\langle p_1^{\mp}| + |p_1^{\pm}\rangle\langle p_5^{\pm}|] \quad \text{for } q + \bar{q} \rightarrow l^+l^- + G. \quad (9)$$

At high energies, both the virtual photon and Z boson contribute to the lepton pair production. The helicity amplitudes are listed in Appendix A. From the amplitudes, we can obtain the polarized parton differential cross sections as follows:

$$\begin{aligned}
d\hat{\sigma}^{(++)} \pm d\hat{\sigma}^{(+-)} &\propto (|M(++; + - +)|^2 + |M(++; - + +)|^2 \\
&\quad \pm |M(+--; + - -)|^2 \pm |M(+--; - + -)|^2)_{\text{fig.1a,1b}} \\
&\quad \pm (|M(+--; + - +)|^2 + |M(+--; - + +)|^2 \\
&\quad + |M(+--; + - -)|^2 + |M(+--; - + -)|^2)_{\text{fig.1c,1d}},
\end{aligned}$$

$$\begin{aligned}
d\hat{\sigma}^{(+)} \pm d\hat{\sigma}^{(-)} &\propto (|M(++; + - +)|^2 + |M(++; - + +)|^2 \\
&\quad + |M(+--; + - -)|^2 + |M(+--; - + -)|^2 \\
&\quad \pm |M(-+; + - +)|^2 \pm |M(-+; - + +)|^2 \\
&\quad \pm |M(--; + - -)|^2 \pm |M(--; - + -)|^2)_{\text{fig.1a,1b}} \\
&\quad + (|M(+--; + - +)|^2 + |M(+--; + - -)|^2 \\
&\quad + |M(+--; - + +)|^2 + |M(+--; - + -)|^2 \\
&\quad \pm |M(-+; + - -)|^2 \pm |M(-+; + - +)|^2 \\
&\quad \pm |M(-+; - + +)|^2 \pm |M(-+; - + -)|^2)_{\text{fig.1c,1d}}.
\end{aligned}$$

To write the differential cross sections explicitly, we consider the center-of-mass frame of the incoming hadrons with momenta

$$P_1 = \frac{1}{2}\sqrt{S}(1, 0, 0, 1), \quad P_2 = \frac{1}{2}\sqrt{S}(1, 0, 0, -1). \quad (10)$$

Let the momentum of the virtual photon or Z boson be q . Then the Mandelstam invariants are:

$$\begin{aligned}
S &= (P_1 + P_2)^2, \\
T &= (q - P_2)^2, \\
U &= (q - P_1)^2.
\end{aligned}
\tag{11}$$

At the parton-level scattering processes, the parton momenta have the explicit forms:

$$\begin{aligned}
p_1 &= x_1 P_1, \\
p_2 &= x_2 P_2, \\
p_5^\mu &= p_1^\mu + p_2^\mu - Q^\mu, \\
Q^\mu &= p_3^\mu + p_4^\mu, \\
q^\mu &= p_4^\mu - p_3^\mu,
\end{aligned}
\tag{12}$$

where p_5 is the momentum of the outgoing parton. The Mandelstam invariants are:

$$\begin{aligned}
\hat{s} &= (p_1 + p_2)^2 = x_1 x_2 S, \\
\hat{t} &= (p_5 - p_2)^2 = (Q - p_1)^2, \\
\hat{u} &= (p_5 - p_1)^2 = (Q - p_2)^2.
\end{aligned}
\tag{13}$$

In the center-of-mass frame of incoming partons, the absolute squares of the *sum of the helicity amplitudes* for the subprocesses $G_{\lambda_1}(p_1) + q_{\lambda_2}(p_2) \rightarrow$

$l_{\lambda_3}^+(p_3) l_{\lambda_4}^-(p_4) + q_{\lambda_5}(p_5)$ are (cf. Appendix B):

$$\begin{aligned}
|M(++; + - +)|_{\text{fig.1a,1b}}^2 &= \left(\frac{2g^2 g_Z^4 R_q^2 L_e^2}{[(q^2 - M_Z^2)^2 + M_Z^2 \Gamma_Z^2]} + \frac{8g^2 e^4 Q_q^2}{q^4} \right. \\
&\quad \left. + \frac{8g^2 g_Z^2 e^2 Q_q R_q L_e (q^2 - M_Z^2)}{q^2 [(q^2 - M_Z^2)^2 + M_Z^2 \Gamma_Z^2]} \right) \left[\frac{2\pi}{\hat{s}} \hat{t}^2 \right. \\
&\quad \left. + \frac{\pi}{\hat{s}} \hat{t} \hat{u} + \pi \hat{u} + 2\pi Q^2 + \frac{\pi}{\hat{s}} \hat{u}^2 \right. \\
&\quad \left. + \frac{\pi}{3} \frac{(Q^2 \hat{t} - \hat{s} \hat{u})}{\hat{s} \hat{u} (\hat{s} - Q^2)^2} (-Q^2 \hat{u} \hat{t} - Q^2 \hat{t}^2 \right. \\
&\quad \left. + \hat{s} \hat{t} \hat{u} + Q^2 \hat{s} \hat{t} - \hat{s}^2 \hat{u} - \hat{s} \hat{u}^2) \right. \\
&\quad \left. + \frac{4\pi}{3} \frac{Q^2 (-\hat{s} \hat{t} + \hat{u} \hat{t} + \hat{t}^2)}{(\hat{s} - Q^2)^2} \right], \quad (14)
\end{aligned}$$

$$|M(++; - + +)|_{\text{fig.1a,1b}}^2 = |M(++; + - +)|_{\text{fig.1a,1b}}^2, \quad (15)$$

$$\begin{aligned}
|M(+ - ; + - -)|_{\text{fig.1a,1b}}^2 &= \left(\frac{2g^2 g_Z^4 L_q^2 L_e^2}{[(q^2 - M_Z^2)^2 + M_Z^2 \Gamma_Z^2]} + \frac{8g^2 e^4 Q_q^2}{q^4} \right. \\
&\quad \left. + \frac{8g^2 g_Z^2 e^2 Q_q L_q L_e (q^2 - M_Z^2)}{q^2 [(q^2 - M_Z^2)^2 + M_Z^2 \Gamma_Z^2]} \right) \times \\
&\quad \left[-\frac{4\pi Q^2}{\hat{s} \hat{u}} \left(\frac{\hat{t}}{2} + \frac{\hat{u}}{2} + Q^2 \right)^2 \right. \\
&\quad \left. - \frac{\pi Q^2}{3 \hat{s} \hat{u} (\hat{s} - Q^2)^2} (Q^2 \hat{u} - \hat{s} \hat{t} \right. \\
&\quad \left. + Q^2 \hat{t} - \hat{s} \hat{u})^2 \right], \quad (16)
\end{aligned}$$

$$|M(+ - ; - + -)|_{\text{fig.1a,1b}}^2 \stackrel{R_e \leftrightarrow L_e}{=} |M(+ - ; + - -)|_{\text{fig.1a,1b}}^2. \quad (17)$$

While for the subprocesses $q_{\lambda_1}(p_1) + \bar{q}_{\lambda_2}(p_2) \rightarrow l_{\lambda_3}^+(p_3) l_{\lambda_4}^-(p_4) + G_{\lambda_5}(p_5)$, the

absolute squares of the *sum of the helicity amplitudes* read

$$\begin{aligned}
|M(+--;+-+)|_{\text{fig.1c,1d}}^2 &= \left(\frac{2g^2g_Z^4L_q^2L_e^2}{[(q^2-M_Z^2)^2+M_Z^2\Gamma_Z^2]} + \frac{8g^2e^4Q_q^2}{q^4} \right. \\
&\quad \left. + \frac{8g^2g_Z^2e^2Q_qL_qL_e(q^2-M_Z^2)}{q^2[(q^2-M_Z^2)^2+M_Z^2\Gamma_Z^2]} \right) \times \\
&\quad \left[\pi Q^2 \frac{\hat{t}}{\hat{u}} + \frac{\pi}{3} \frac{Q^2(Q^2\hat{u}-\hat{s}\hat{t})^2}{\hat{u}\hat{t}(\hat{s}-Q^2)^2} \right. \\
&\quad \left. + \frac{4\pi}{3} \frac{Q^4\hat{s}}{(\hat{s}-Q^2)^2} \right], \tag{18}
\end{aligned}$$

$$|M(+--;-++)|_{\text{fig.1c,1d}}^2 \stackrel{R_e \leftrightarrow L_e}{=} |M(+--;+-+)|_{\text{fig.1c,1d}}^2, \tag{19}$$

$$\begin{aligned}
|M(+--;+--)|_{\text{fig.1c,1d}}^2 &= \left(\frac{2g^2g_Z^4L_q^2L_e^2}{[(q^2-M_Z^2)^2+M_Z^2\Gamma_Z^2]} + \frac{8g^2e^4Q_q^2}{q^4} \right. \\
&\quad \left. + \frac{8g^2g_Z^2e^2Q_qL_qL_e(q^2-M_Z^2)}{q^2[(q^2-M_Z^2)^2+M_Z^2\Gamma_Z^2]} \right) \times \\
&\quad \left[-2\pi\hat{u} - 2\pi Q^2 - \pi \frac{\hat{s}\hat{u}}{\hat{t}} - 2\pi Q^2 \frac{\hat{s}}{\hat{t}} \right. \\
&\quad \left. + \frac{2\pi}{3} \frac{(Q^2\hat{t}-\hat{s}\hat{u})^2}{\hat{u}(\hat{s}-Q^2)^2} + \frac{\pi}{3} \frac{\hat{s}(Q^2\hat{t}-\hat{u}\hat{s})^2}{\hat{u}\hat{t}(\hat{s}-Q^2)^2} \right. \\
&\quad \left. + \frac{4\pi}{3} \frac{Q^2\hat{s}\hat{t}}{(\hat{s}-Q^2)^2} + \frac{4\pi}{3} \frac{Q^2\hat{s}^2}{(\hat{s}-Q^2)^2} \right], \tag{20}
\end{aligned}$$

$$|M(+--;-+-)|_{\text{fig.1c,1d}}^2 \stackrel{R_e \leftrightarrow L_e}{=} |M(+--;+--)|_{\text{fig.1c,1d}}^2. \tag{21}$$

III. Numerical Results

In this section, the differential cross sections for the polarized processes

will be calculated numerically. For the double polarized hadron process, we have

$$\frac{d\Delta\sigma}{dQ^2 dy dq_T^2} = \sum_{ij} \int dx_1 dx_2 \Delta f_i(x_1) \Delta f_j(x_2) [\hat{s} \frac{d\Delta\hat{\sigma}_{ij}}{dQ^2 d\hat{t} d\hat{u}}], \quad (22)$$

where y is the rapidity,

$$\Delta f_i(x) = f_i^{(+)}(x) - f_i^{(-)}(x), \quad (23)$$

is the polarized structure function, and

$$d\Delta\hat{\sigma}_{ij} = \frac{1}{2}(d\hat{\sigma}_{ij}^{(++)} - d\hat{\sigma}_{ij}^{(+-)}). \quad (24)$$

For the single polarized hadron process, we have

$$\frac{d\Delta\sigma}{dQ^2 dy dq_T^2} = \sum_{ij} \int dx_1 dx_2 \Delta f_i(x_1) f_j(x_2) [\hat{s} \frac{d\Delta\hat{\sigma}_{ij}}{dQ^2 d\hat{t} d\hat{u}}], \quad (25)$$

$$\begin{aligned} d\Delta\hat{\sigma}_{ij} &= d\hat{\sigma}_{ij}^{(+)} - d\hat{\sigma}_{ij}^{(-)} \\ &= \frac{1}{2}(d\hat{\sigma}_{ij}^{(++)} + d\hat{\sigma}_{ij}^{(+-)} - d\hat{\sigma}_{ij}^{(-+)} - d\hat{\sigma}_{ij}^{(--)}). \end{aligned} \quad (26)$$

In the rest frame of $\gamma^*(Z^0)$ [10], the momenta of the lepton pair and outgoing parton are:

$$\begin{aligned} p_3^\mu &= \frac{1}{2}(E' - q' \cos \alpha, q' \sin \theta - q \sin \alpha \cos \beta \cos \theta - E' \cos \alpha \sin \theta, \\ &\quad -q \sin \alpha \sin \beta, q' \cos \theta - E' \cos \alpha \cos \theta + q \sin \alpha \cos \beta \sin \theta), \\ p_4^\mu &= \frac{1}{2}(E' + q' \cos \alpha, q' \sin \theta + q \sin \alpha \cos \beta \cos \theta + E' \cos \alpha \sin \theta, \\ &\quad q \sin \alpha \sin \beta, q' \cos \theta + E' \cos \alpha \cos \theta - q \sin \alpha \cos \beta \sin \theta), \\ p_5^\mu &= (q', -q' \sin \theta, 0, -q' \cos \theta), \end{aligned} \quad (27)$$

where $E' = \frac{\hat{s}+q^2}{2\sqrt{\hat{s}}}$ and $q' = \frac{\hat{s}-q^2}{2\sqrt{\hat{s}}}$. The above momenta are in the form $x^\mu = (t, x, y, z)$. The momenta of the incident partons thus define the z axis and the direction of the $\gamma^*(Z^0)$ defines the x - z plane. The angles α and β describe the decay of the $\gamma^*(Z^0)$ relative to its axes. The phase space integration becomes

$$\begin{aligned} \frac{1}{(2\pi)^5} \frac{d^3p_3}{2p_3^0} \frac{d^3p_4}{2p_4^0} \frac{d^3p_5}{2p_5^0} \delta^4(p_1 + p_2 - q - p_5) \\ = \frac{1}{(2\pi)^5} \frac{1}{16} d\Omega \pi \delta(\hat{s} + \hat{t} + \hat{u} - Q^2) \left(\frac{dQ^2 d\hat{t} d\hat{u}}{\hat{s}} \right). \end{aligned} \quad (28)$$

To calculate the differential cross sections at the hadron level, we write the (double polarized) differential cross section as [11]

$$\begin{aligned} \frac{d\Delta\sigma}{dQ^2 dy dq_T^2} &= \sum_{ij} \int dx_1 dx_2 \Delta f(x_1) \Delta f(x_2) \left[\hat{s} \frac{d\Delta\hat{\sigma}_{ij}}{dQ^2 d\hat{t} d\hat{u}} \right] \\ &\equiv \int dx_1 dx_2 \delta(\hat{s} + \hat{t} + \hat{u} - Q^2) f(x_1, x_2) \\ &\equiv \int_{\sqrt{\tau_+} e^y}^1 \frac{dx_1 f(x_1, x_2^*)}{x_1 S - \sqrt{\hat{s}}(Q^2 + q_T^2)^{\frac{1}{2}} e^y} \\ &\quad + \int_{\sqrt{\tau_+} e^{-y}}^1 \frac{dx_2 f(x_1^*, x_2)}{x_2 S - \sqrt{\hat{s}}(Q^2 + q_T^2)^{\frac{1}{2}} e^{-y}}, \end{aligned} \quad (29)$$

where

$$\sqrt{\tau_+} = \sqrt{\frac{q_T^2}{S}} + \sqrt{\tau + \frac{q_T^2}{S}}; \quad \tau = \frac{Q^2}{S}, \quad (30)$$

and

$$x_1^* = \frac{x_2 \sqrt{S}(Q^2 + q_T^2)^{\frac{1}{2}} e^{-y} - Q^2}{x_2 S - \sqrt{S}(Q^2 + q_T^2)^{\frac{1}{2}} e^y}, \quad (31)$$

$$x_2^* = \frac{x_1 \sqrt{S}(Q^2 + q_T^2)^{\frac{1}{2}} e^y - Q^2}{x_1 S - \sqrt{S}(Q^2 + q_T^2)^{\frac{1}{2}} e^{-y}}. \quad (32)$$

Finally, we evaluate the single-spin and double-spin asymmetries defined respectively as:

$$A_L = \frac{d\sigma^{(+)} - d\sigma^{(-)}}{d\sigma^{(+)} + d\sigma^{(-)}}, \quad (33)$$

$$A_{LL} = \frac{d\sigma^{(++)} - d\sigma^{(+-)}}{d\sigma^{(++)} + d\sigma^{(+-)}}. \quad (34)$$

To evaluate A_{LL} , we need polarized parton distribution functions, which we shall use those given by Cheng, *et al.* (CLW) [12] and those by Glück, *et al.* (GRSV) [13]. To obtain A_L , we need to use polarized parton distribution functions together with the corresponding unpolarized ones. Specifically, the CLW sets should be used with the MRS(A') sets [14], while the GRSV sets should be used with the unpolarized GRV sets [15].

In the CLW sets, two different cases of polarized parton distributions in the gauge-invariant factorization scheme are used: (I) sea polarization $\Delta s(x) \neq 0$, gluon polarization $\Delta G(x) = 0$; and (II) $\Delta s(x) \neq 0, \Delta G(x) \neq 0$, where in both cases $\Delta u(x) = \Delta d(x) = \Delta s(x)$ is assumed. Here the spin-dependent Altarelli-Parisi equations are applied directly to the gauge-invariant parton spin distributions.

While in the GRSV sets, polarized deep inelastic lepton nucleon scattering was considered up to the next-to-leading order QCD within the framework of the radiative parton model. The structure functions were subject to two different sets of theoretical constraints related to two different views concerning the flavor $SU_f(3)$ symmetry properties of hyperon β -decays [16].

One set is called the standard (ST) scenario, while the other set is called the valence (VA) scenario.

Figure 2 shows the unpolarized differential cross sections being plotted with q_T and $\sqrt{S} = 500\text{GeV}$. Three different dilepton masses of $Q = 10\text{GeV}$, $Q = 50\text{GeV}$ and $Q = M_Z$ are used. The MRS(A') and the GRV sets, which are defined up to the next-to-leading order in QCD, give essentially the same results.

Figures 3a–3c and 4a–4c show the predictions for the single-spin asymmetries and double-spin asymmetries, respectively. From Fig. 3a–3c, we note that the two CLW sets generally give larger differences between the single-spin asymmetries $|A_L|$ than the two GRSV sets. The differences between the asymmetries from the two GRSV sets are essentially constant over the given q_T range. The asymmetries from both the CLW and GRSV sets are large when the dilepton mass is equal to M_Z , due to the fact that the effects of the Z interference become important when the dilepton mass is equal to M_Z . From $Q = 10\text{GeV}$ to $Q = M_Z$, the asymmetries change by two orders of magnitude.

From Fig. 4a–4c, the double-spin asymmetries $|A_{LL}|$ are of the same order of magnitude in the given q_T range and for the three Q values. The CLW sets give comparatively larger differences between the asymmetries in the same q_T range than the GRSV sets, which give essentially the same differences between the asymmetries.

Finally, in Fig. 5a-5d, we give the contributions of the subprocesses $G + q \rightarrow l^+l^- + q$ (Fig. 1a-1b) and $q + \bar{q} \rightarrow l^+l^- + G$ (Fig. 1c-1d) to the single-spin and double-spin asymmetries at $Q = M_Z$ and $\sqrt{S} = 500\text{GeV}$. Fig. 5a-5b are obtained from the CLW sets, while Fig. 5c-5d are obtained from the GRSV sets. We observe that quark-gluon and quark-quark contributions to the single-spin and double-spin asymmetries behave differently with increasing q_T . The contributions of the subprocesses to the asymmetries obtained from the CLW sets are more dispersed and are larger than those from the GRSV sets, while the single-spin or double-spin asymmetries of the subprocesses obtained from the two GRSV sets have similar behavior. In general, the contributions from quark-gluon (Fig. 1a-1b) vary more significantly than that from quarks (Fig 1c-1d) alone.

IV. Conclusion

In this paper, we have made a numerical study of the single-spin and double-spin asymmetries for the $PP \rightarrow l^+l^- + jet$ process. In this study, we have used, for convenience, the helicity amplitude method to calculate the scattering amplitudes and the differential cross sections for the asymmetries. Both the asymmetries of the angular distribution of lepton pair in the large transverse momentum Drell-Yan process at RHIC energies were studied. Polarized parton distributions from CLW [12] and from GRSV [13] were used. Both the CLW and the GRSV sets were obtained to the

next-to-leading order. We have used the MRS(A') [14] and the GRV [15] sets of unpolarized distribution functions, which are also given to the next-to-leading order. The unpolarized differential cross sections obtained from these sets are essentially the same.

We observe that the two CLW sets generally give larger differences between the single-spin asymmetries $|A_L|$ than the two GRSV sets, and the asymmetries generally increase as the dilepton mass approaches M_Z , due to the large effects of the Z interference from the parity-violating Z -fermion coupling. The differences between the asymmetries from the two GRSV sets are essentially constant and small. From $Q = 10\text{GeV}$ to $Q = M_Z$, the asymmetries change by two orders of magnitude.

However, the double-spin asymmetries $|A_{LL}|$ are of the same order of magnitude in the same q_T range and for the three Q values. The CLW sets give comparatively larger differences between the asymmetries for the same q_T range than the GRSV sets, which give essentially constant differences between the asymmetries. We note that the asymmetries are nearly constant for different Q values.

We have also calculated the contributions of the subprocesses $G + q \rightarrow l^+l^- + q$ (Fig. 1a-1b) and $q + \bar{q} \rightarrow l^+l^- + G$ (Fig. 1c-1d) to the single-spin and double-spin asymmetries at $Q = M_Z$ and $\sqrt{S} = 500\text{GeV}$. The single-spin and double-spin asymmetries behave differently with increasing q_T . The asymmetries of the subprocesses obtained from the CLW sets are

more dispersed than from the GRSV sets, while those obtained from the two GRSV sets have similar behavior.

We observe that, at high energies, Z boson contributes significantly to the polarized process and induces large parity-violating single-spin asymmetries. The single-spin asymmetries become large as the dilepton mass approaches the Z peak for both the CLW and GRSV sets. The double-spin asymmetries are generally larger than the single-spin asymmetries for any dilepton mass. Therefore, measurements of the single-spin asymmetries may be used to pin down the spin structure of the proton for distinguishing the two CLW sets. However, the two GRSV sets give about the same results over large values of q_T for different dilepton masses.

Finally, we should mention that Leader and Srihedar [17] have also made a detailed study on the polarized $PP \rightarrow l^+l^- + jet$ and obtained some similar results. Their work and ours were based on the $O(\alpha_s)$ tree Feynman diagrams on the parton level. One-loop radiative QCD corrections to the polarized parton subprocesses remain to be calculated and are difficult. We note that, for the unpolarized Drell-Yan process, inclusion of the $O(\alpha_s^2)$ corrections changes the cross section at fixed target energies up to 10% [18].

Acknowledgments

This research was supported by the National Science Council of the

Republic of China under Contract Nos. NSC 86-2112-M-006-002 and NSC 86-2112-M-006-005.

Appendix A

Here we list the nonvanishing helicity amplitudes for the polarized hadron subprocesses. With the contribution of a Z boson, the amplitudes read

$$\begin{aligned}
M_1^Z(+, +; +, -, +) &= \frac{\sqrt{2}igT^a g_Z^2 R_q L_e}{(q^2 - M_Z^2 + iM_Z\Gamma_Z)} \frac{\langle 13 \rangle^\dagger \langle 42 \rangle}{\langle 51 \rangle}, \\
M_2^Z(+, +; +, -, +) &= \frac{\sqrt{2}igT^a g_Z^2 R_q L_e}{(q^2 - M_Z^2 + iM_Z\Gamma_Z)} \frac{\langle 52 \rangle \langle 35 \rangle^\dagger \langle 42 \rangle}{\langle 51 \rangle \langle 12 \rangle}, \\
M_1^Z(+, +; -, +, +) &= \frac{\sqrt{2}igT^a g_Z^2 R_q R_e}{(q^2 - M_Z^2 + iM_Z\Gamma_Z)} \frac{\langle 41 \rangle^\dagger \langle 32 \rangle}{\langle 15 \rangle}, \\
M_2^Z(+, +; -, +, +) &= \frac{\sqrt{2}igT^a g_Z^2 R_q R_e}{(q^2 - M_Z^2 + iM_Z\Gamma_Z)} \frac{\langle 52 \rangle \langle 45 \rangle^\dagger \langle 32 \rangle}{\langle 12 \rangle \langle 51 \rangle}, \\
M_2^Z(+, -; +, -, -) &= \frac{\sqrt{2}igT^a g_Z^2 R_q L_e}{(q^2 - M_Z^2 + iM_Z\Gamma_Z)} \frac{\langle 45 \rangle^2 \langle 43 \rangle^\dagger}{\langle 12 \rangle \langle 51 \rangle}, \\
M_2^Z(+, -; -, +, -) &= \frac{\sqrt{2}igT^a g_Z^2 L_q R_e}{(q^2 - M_Z^2 + iM_Z\Gamma_Z)} \frac{\langle 35 \rangle^2 \langle 34 \rangle^\dagger}{\langle 12 \rangle \langle 51 \rangle}, \\
M_2^Z(-, +; +, -, +) &= \frac{\sqrt{2}igT^a g_Z^2 R_q L_e}{(q^2 - M_Z^2 + iM_Z\Gamma_Z)} \frac{\langle 35 \rangle^{\dagger 2} \langle 43 \rangle}{\langle 12 \rangle^\dagger \langle 15 \rangle^\dagger}, \\
M_2^Z(-, +; -, +, +) &= \frac{\sqrt{2}igT^a g_Z^2 R_q R_e}{(q^2 - M_Z^2 + iM_Z\Gamma_Z)} \frac{\langle 45 \rangle^{\dagger 2} \langle 34 \rangle}{\langle 12 \rangle^\dagger \langle 15 \rangle^\dagger}, \\
M_1^Z(-, -; +, -, -) &= \frac{\sqrt{2}igT^a g_Z^2 L_q L_e}{(q^2 - M_Z^2 + iM_Z\Gamma_Z)} \frac{\langle 14 \rangle \langle 23 \rangle^\dagger}{\langle 15 \rangle^\dagger}, \\
M_2^Z(-, -; +, -, -) &= \frac{\sqrt{2}igT^a g_Z^2 L_q L_e}{(q^2 - M_Z^2 + iM_Z\Gamma_Z)} \frac{\langle 25 \rangle^\dagger \langle 54 \rangle \langle 23 \rangle^\dagger}{\langle 12 \rangle^\dagger \langle 15 \rangle^\dagger}, \\
M_1^Z(-, -; -, +, -) &= \frac{\sqrt{2}igT^a g_Z^2 L_q R_e}{(q^2 - M_Z^2 + iM_Z\Gamma_Z)} \frac{\langle 13 \rangle \langle 42 \rangle^\dagger}{\langle 51 \rangle^\dagger},
\end{aligned}$$

$$\begin{aligned}
M_2^Z(-, -; -, +, -) &= \frac{\sqrt{2}igT^a g_Z^2 L_q R_e}{(q^2 - M_Z^2 + iM_Z\Gamma_Z)} \frac{\langle 24 \rangle^\dagger \langle 53 \rangle \langle 25 \rangle^\dagger}{\langle 12 \rangle^\dagger \langle 15 \rangle^\dagger}, \\
M_4^Z(+, -; +, -, +) &= \frac{\sqrt{2}igT^a g_Z^2 L_q L_e}{(q^2 - M_Z^2 + iM_Z\Gamma_Z)} \frac{\langle 14 \rangle^2 \langle 43 \rangle^\dagger}{\langle 15 \rangle \langle 25 \rangle}, \\
M_3^Z(+, -; +, -, -) &= \frac{\sqrt{2}igT^a g_Z^2 L_q L_e}{(q^2 - M_Z^2 + iM_Z\Gamma_Z)} \frac{\langle 23 \rangle^\dagger \langle 54 \rangle}{\langle 15 \rangle^\dagger}, \\
M_4^Z(+, -; +, -, -) &= \frac{\sqrt{2}igT^a g_Z^2 L_q L_e}{(q^2 - M_Z^2 + iM_Z\Gamma_Z)} \frac{\langle 21 \rangle^\dagger \langle 14 \rangle \langle 23 \rangle^\dagger}{\langle 25 \rangle^\dagger \langle 51 \rangle^\dagger}, \\
M_4^Z(+, -; -, +, +) &= \frac{\sqrt{2}igT^a g_Z^2 L_q R_e}{(q^2 - M_Z^2 + iM_Z\Gamma_Z)} \frac{\langle 13 \rangle^2 \langle 34 \rangle^\dagger}{\langle 25 \rangle \langle 15 \rangle}, \\
M_3^Z(+, -; -, +, -) &= \frac{\sqrt{2}igT^a g_Z^2 L_q R_e}{(q^2 - M_Z^2 + iM_Z\Gamma_Z)} \frac{\langle 53 \rangle \langle 24 \rangle^\dagger}{\langle 15 \rangle^\dagger}, \\
M_4^Z(+, -; -, +, -) &= \frac{\sqrt{2}igT^a g_Z^2 L_q R_e}{(q^2 - M_Z^2 + iM_Z\Gamma_Z)} \frac{\langle 13 \rangle \langle 24 \rangle^\dagger \langle 21 \rangle^\dagger}{\langle 25 \rangle^\dagger \langle 51 \rangle^\dagger}, \\
M_3^Z(+, -; +, -, +) &= \frac{\sqrt{2}igT^a g_Z^2 R_q L_e}{(q^2 - M_Z^2 + iM_Z\Gamma_Z)} \frac{\langle 42 \rangle \langle 35 \rangle^\dagger}{\langle 15 \rangle}, \\
M_4^Z(-, +; +, -, +) &= \frac{\sqrt{2}igT^a g_Z^2 R_q L_e}{(q^2 - M_Z^2 + iM_Z\Gamma_Z)} \frac{\langle 42 \rangle \langle 31 \rangle^\dagger \langle 12 \rangle}{\langle 25 \rangle \langle 15 \rangle}, \\
M_4^Z(-, +; +, -, -) &= \frac{\sqrt{2}igT^a g_Z^2 R_q L_e}{(q^2 - M_Z^2 + iM_Z\Gamma_Z)} \frac{\langle 13 \rangle^{\dagger 2} \langle 43 \rangle}{\langle 25 \rangle^\dagger \langle 51 \rangle^\dagger}, \\
M_3^Z(-, +; -, +, +) &= \frac{\sqrt{2}igT^a g_Z^2 R_q R_e}{(q^2 - M_Z^2 + iM_Z\Gamma_Z)} \frac{\langle 32 \rangle \langle 45 \rangle^\dagger}{\langle 15 \rangle}, \\
M_4^Z(-, +; -, +, +) &= \frac{\sqrt{2}igT^a g_Z^2 R_q R_e}{(q^2 - M_Z^2 + iM_Z\Gamma_Z)} \frac{\langle 12 \rangle \langle 41 \rangle^\dagger \langle 32 \rangle}{\langle 25 \rangle \langle 15 \rangle}, \\
M_4^Z(-, +; -, +, -) &= \frac{\sqrt{2}igT^a g_Z^2 R_q R_e}{(q^2 - M_Z^2 + iM_Z\Gamma_Z)} \frac{\langle 14 \rangle^{\dagger 2} \langle 34 \rangle}{\langle 25 \rangle^\dagger \langle 51 \rangle^\dagger}.
\end{aligned} \tag{35}$$

The parameters $L_q = 2\tau_3 - 2Q_q \sin^2 \theta_W$, $R_q = -2Q_q \sin^2 \theta_W$ are, respectively, the left-handed and right-handed coupling constants, of quark coupled with the Z boson, where τ_3 is an $SU(2)$ isospin quantum number, Q_q is the charge

of the quark, θ_W is the Weinberg angle, and T^a is the $SU(3)$ generator with a being the color index.

With the contribution of a virtual photon, we have

$$\begin{aligned}
M_1^\gamma(+, +; +, -, +) &= \frac{2\sqrt{2}ige^2 Q_q T^a}{q^2} \frac{\langle 31 \rangle^\dagger \langle 42 \rangle}{\langle 15 \rangle}, \\
M_2^\gamma(+, +; +, -, +) &= \frac{2\sqrt{2}ige^2 Q_q T^a}{q^2} \frac{\langle 52 \rangle \langle 35 \rangle^\dagger \langle 42 \rangle}{\langle 51 \rangle \langle 12 \rangle}, \\
M_1^\gamma(+, +; -, +, +) &= \frac{2\sqrt{2}ige^2 Q_q T^a}{q^2} \frac{\langle 41 \rangle^\dagger \langle 32 \rangle}{\langle 15 \rangle}, \\
M_2^\gamma(+, +; -, +, +) &= \frac{2\sqrt{2}ige^2 Q_q T^a}{q^2} \frac{\langle 52 \rangle \langle 45 \rangle^\dagger \langle 32 \rangle}{\langle 12 \rangle \langle 51 \rangle}, \\
M_2^\gamma(+, -; +, -, -) &= \frac{2\sqrt{2}ige^2 Q_q T^a}{q^2} \frac{\langle 45 \rangle^2 \langle 43 \rangle^\dagger}{\langle 12 \rangle \langle 51 \rangle}, \\
M_2^\gamma(+, -; -, +, -) &= \frac{2\sqrt{2}ige^2 Q_q T^a}{q^2} \frac{\langle 35 \rangle^2 \langle 34 \rangle^\dagger}{\langle 12 \rangle \langle 51 \rangle}, \\
M_2^\gamma(-, +; +, -, +) &= \frac{2\sqrt{2}ige^2 Q_q T^a}{q^2} \frac{\langle 35 \rangle^\dagger{}^2 \langle 43 \rangle}{\langle 12 \rangle^\dagger \langle 15 \rangle^\dagger}, \\
M_2^\gamma(-, +; -, +, +) &= \frac{2\sqrt{2}ige^2 Q_q T^a}{q^2} \frac{\langle 45 \rangle^\dagger{}^2 \langle 34 \rangle}{\langle 12 \rangle^\dagger \langle 15 \rangle^\dagger}, \\
M_1^\gamma(-, -; +, -, -) &= \frac{2\sqrt{2}ige^2 Q_q T^a}{q^2} \frac{\langle 14 \rangle \langle 23 \rangle^\dagger}{\langle 15 \rangle^\dagger}, \\
M_2^\gamma(-, -; +, -, -) &= \frac{2\sqrt{2}ige^2 Q_q T^a}{q^2} \frac{\langle 25 \rangle^\dagger \langle 54 \rangle \langle 23 \rangle^\dagger}{\langle 12 \rangle^\dagger \langle 15 \rangle^\dagger}, \\
M_1^\gamma(-, -; -, +, -) &= \frac{2\sqrt{2}ige^2 Q_q T^a}{q^2} \frac{\langle 13 \rangle \langle 24 \rangle^\dagger}{\langle 15 \rangle^\dagger}, \\
M_2^\gamma(-, -; -, +, -) &= \frac{2\sqrt{2}ige^2 Q_q T^a}{q^2} \frac{\langle 24 \rangle^\dagger \langle 53 \rangle \langle 25 \rangle^\dagger}{\langle 12 \rangle^\dagger \langle 15 \rangle^\dagger}, \\
M_4^\gamma(+, -; +, -, +) &= \frac{2\sqrt{2}ige^2 Q_q T^a}{q^2} \frac{\langle 14 \rangle^2 \langle 43 \rangle^\dagger}{\langle 25 \rangle \langle 15 \rangle}, \\
M_3^\gamma(+, -; +, -, -) &= \frac{2\sqrt{2}ige^2 Q_q T^a}{q^2} \frac{\langle 54 \rangle \langle 23 \rangle^\dagger}{\langle 15 \rangle^\dagger},
\end{aligned}$$

$$\begin{aligned}
M_4^\gamma(+, -; +, -, -) &= \frac{2\sqrt{2}ige^2 Q_q T^a}{q^2} \frac{\langle 14 \rangle \langle 23 \rangle^\dagger \langle 21 \rangle^\dagger}{\langle 25 \rangle^\dagger \langle 51 \rangle^\dagger}, \\
M_4^\gamma(+, -; -, +, +) &= \frac{2\sqrt{2}ige^2 Q_q T^a}{q^2} \frac{\langle 13 \rangle^2 \langle 34 \rangle^\dagger}{\langle 15 \rangle \langle 25 \rangle}, \\
M_3^\gamma(+, -; -, +, -) &= \frac{2\sqrt{2}ige^2 Q_q T^a}{q^2} \frac{\langle 53 \rangle \langle 24 \rangle^\dagger}{\langle 15 \rangle^\dagger}, \\
M_4^\gamma(+, -; -, +, -) &= \frac{2\sqrt{2}ige^2 Q_q T^a}{q^2} \frac{\langle 21 \rangle^\dagger \langle 24 \rangle^\dagger \langle 13 \rangle}{\langle 25 \rangle^\dagger \langle 51 \rangle^\dagger}, \\
M_3^\gamma(-, +; +, -, +) &= \frac{2\sqrt{2}ige^2 Q_q T^a}{q^2} \frac{\langle 42 \rangle \langle 35 \rangle^\dagger}{\langle 15 \rangle}, \\
M_4^\gamma(-, +; +, -, +) &= \frac{2\sqrt{2}ige^2 Q_q T^a}{q^2} \frac{\langle 12 \rangle \langle 42 \rangle \langle 31 \rangle^\dagger}{\langle 15 \rangle \langle 25 \rangle}, \\
M_4^\gamma(-, +; +, -, -) &= \frac{2\sqrt{2}ige^2 Q_q T^a}{q^2} \frac{\langle 13 \rangle^{\dagger 2} \langle 43 \rangle}{\langle 15 \rangle^\dagger \langle 25 \rangle^\dagger}, \\
M_3^\gamma(-, +; -, +, +) &= \frac{2\sqrt{2}ige^2 Q_q T^a}{q^2} \frac{\langle 32 \rangle \langle 45 \rangle^\dagger}{\langle 15 \rangle}, \\
M_4^\gamma(-, +; -, +, +) &= \frac{2\sqrt{2}ige^2 Q_q T^a}{q^2} \frac{\langle 41 \rangle^\dagger \langle 32 \rangle \langle 12 \rangle}{\langle 25 \rangle \langle 15 \rangle}, \\
M_4^\gamma(-, +; -, +, -) &= \frac{2\sqrt{2}ige^2 Q_q T^a}{q^2} \frac{\langle 14 \rangle^{\dagger 2} \langle 34 \rangle}{\langle 25 \rangle^\dagger \langle 51 \rangle^\dagger}.
\end{aligned}$$

Appendix B

In this appendix, we list the relations between the invariant variables s_{ij} and the Mandelstam invariants.

$$\begin{aligned}
s_{12} &= \hat{s} \\
s_{13} &= 2p_1 \cdot p_3 \\
&= \frac{1}{2}(Q^2 - \hat{t}) - \frac{Q^2 \hat{u} - \hat{s} \hat{t}}{2(\hat{s} - Q^2)} \cos \alpha - \frac{\sqrt{Q^2 \hat{s} \hat{t} \hat{u}}}{\hat{s} - Q^2} \sin \alpha \cos \beta
\end{aligned}$$

$$\begin{aligned}
s_{14} &= 2p_1 \cdot p_4 \\
&= \frac{1}{2}(Q^2 - \hat{t}) + \frac{Q^2 \hat{u} - \hat{s} \hat{t}}{2(\hat{s} - Q^2)} \cos \alpha + \frac{\sqrt{Q^2 \hat{s} \hat{t} \hat{u}}}{\hat{s} - Q^2} \sin \alpha \cos \beta \\
s_{15} &= 2p_1 \cdot p_5 = -\hat{u} \\
s_{23} &= 2p_2 \cdot p_3 \\
&= \frac{1}{2}(Q^2 - \hat{u}) - \frac{Q^2 \hat{t} - \hat{s} \hat{u}}{2(\hat{s} - Q^2)} \cos \alpha + \frac{\sqrt{Q^2 \hat{s} \hat{t} \hat{u}}}{\hat{s} - Q^2} \sin \alpha \cos \beta \\
s_{24} &= 2p_2 \cdot p_4 \\
&= \frac{1}{2}(Q^2 - \hat{u}) + \frac{Q^2 \hat{t} - \hat{s} \hat{u}}{2(\hat{s} - Q^2)} \cos \alpha - \frac{\sqrt{Q^2 \hat{s} \hat{t} \hat{u}}}{\hat{s} - Q^2} \sin \alpha \cos \beta \\
s_{25} &= 2p_2 \cdot p_5 = -\hat{t} \\
s_{34} &= 2p_3 \cdot p_4 = Q^2 \\
s_{35} &= 2p_3 \cdot p_5 = -\frac{\hat{u} + \hat{t}}{2}(1 - \cos \alpha) \\
s_{45} &= 2p_4 \cdot p_5 = -\frac{\hat{u} + \hat{t}}{2}(1 + \cos \alpha) .
\end{aligned}$$

References

- [1] J. Ashman, *et al.* (EMC), Phys. Lett. **B206** (1988) 364; Nucl. Phys. **B328** (1989) 1.
- [2] D. Adams, *et al.* SMC, Phys. Lett. **B302** (1993) 533; **B329** (1994) 399; **B339(E)** (1994) 332; Phys. Lett. **B357** (1995) 248.
- [3] D.L. Anthony, *et al.* E142, Phys. Rev. Lett. **71** (1993) 959.
- [4] K. Abe, *et al.* E143, Phys. Rev. Lett. **74** (1995) 346; **75** (1995) 25.

- [5] R.L. Jaffe and A. Manohar, Nucl. Phys. **B337** (1990) 509.
- [6] G. Altarelli and G.G. Ross, Phys. Lett. **B212** (1988) 883; R. Carlitz, J. Collins and A. Mueller, Phys. Lett. **B214** (1988) 229; A. Efremov and O. Teryaev, Phys. Lett. **B240** (1990) 373.
- [7] H.-Y. Cheng and C.-F. Wai, Phys. Rev. **D46** (1992) 125.
- [8] H.-Y. Cheng, M. Huang and C.-F. Wai, Phys. Rev. **D49** (1994) 1272.
- [9] P. De Causmaecker, R. Gastmans, W. Troost and T.T. Wu, Phys. Lett. **B105** (1981) 215; D. Danckaert, P. De Causmaecker, R. Gastmans, W. Troost and T.T. Wu, Phys. Lett. **B114** (1982) 203; P. De Causmaecker, R. Gastmans, W. Troost and T.T. Wu, Nucl. Phys. **B206** (1982) 53; F.A. Berends, R. Kleiss, P. De Causmaecker, R. Gastmans, W. Troost and T.T. Wu, Nucl. Phys. **B206** (1982) 61; **B239** (1984) 382, 395.
- [10] R.D. Carlitz and R.S. Willey, Phys. Rev. **D45** (1992) 2323.
- [11] G. Altarelli, R.K. Ellis and G. Martinelli, Nucl. Phys. **B157** (1979) 461.
- [12] H.-Y. Cheng, H. H. Liu and C.-Y. Wu, Phys. Rev. **D53** (1996) 2380.
- [13] M. Glück, E. Reya, M. Stratmann and W. Vogelsang, Phys. Lett. **B359** (1995) 201; Phys. Rev. **D53** (1996) 4775.

- [14] A.D. Martin, R.G. Roberts and W.J. Stirling, Phys. Rev. **D50** (1994) 6734; Phys. Lett. **B354** (1995) 155.
- [15] M. Glück, E. Reya and A. Vogt, Z. Phys. **C67** (1995) 433.
- [16] H.J. Lipkin, Phys. Lett. **B256** (1991) 284; **B337** (1994) 157;
J. Lichtenstadt and H.J. Lipkin, Phys. Lett. **B353** (1995) 119.
- [17] E. Leader and K. Sridhar, Phys. Lett. **B311** (1993) 324; Nucl. Phys. **B419** (1994) 3.
- [18] P.J. Rijken and W.L. van Neerven, Phys. Rev. **D51** (1995) 44, and references cited therein.

FIGURE CAPTIONS

Fig. 1 Feynman diagrams for the $PP \rightarrow l^+l^- + jet$. Curly lines denote gluons, wavy lines denote γ^* or Z bosons and solid lines denote quarks and lepton pairs.

Fig. 2 Unpolarized differential cross sections for the $PP \rightarrow l^+l^- + jet$ process at $\sqrt{S} = 500GeV$, as a function of q_T , with τ is fixed at Q^2/S and $y = 0$, at various dilepton masses: $Q = 10GeV, 50GeV, M_Z$. The MRS(A') set and the GRV set give essentially the same results.

Fig. 3 Single-spin asymmetries for the $PP \rightarrow l^+l^- + jet$ process at $\sqrt{S} = 500GeV$, as a function of q_T . The asymmetries shown in these figures are constructed out of the cross-sections differential in q_T , rapidity y and τ , with τ being fixed at Q^2/S and $y = 0$. The full and dotted lines correspond respectively to the CLW Set I and Set II, which are used together with the MRS(A') unpolarized distribution functions. The circle-full and dotted-full lines correspond respectively to the GRSV standard (ST) and valence (VA) scenario sets, which are used together with the GRV sets. Three figures corresponding to (a) $Q = 10GeV$, (b) $Q = 50GeV$ and (c) $Q = M_Z$ are shown.

Fig. 4 Double-spin asymmetries for the $PP \rightarrow l^+l^- + jet$ process at $\sqrt{S} = 500GeV$, as a function of q_T . Three figures corresponding to (a) $Q = 10GeV$, (b) $Q = 50GeV$ and (c) $Q = M_Z$ are shown.

Fig. 5 Contributions of the subprocesses $G + q \rightarrow l^+l^- + q$ (Fig. 1a-1b) and $q + \bar{q} \rightarrow l^+l^- + G$ (Fig. 1c-1d) to the single-spin and double-spin asymmetries at $Q = M_Z$ and $\sqrt{S} = 500GeV$. (a) and (b) are contributions obtained from the CLW sets, while (c) and (d) are those obtained from the GRSV sets.

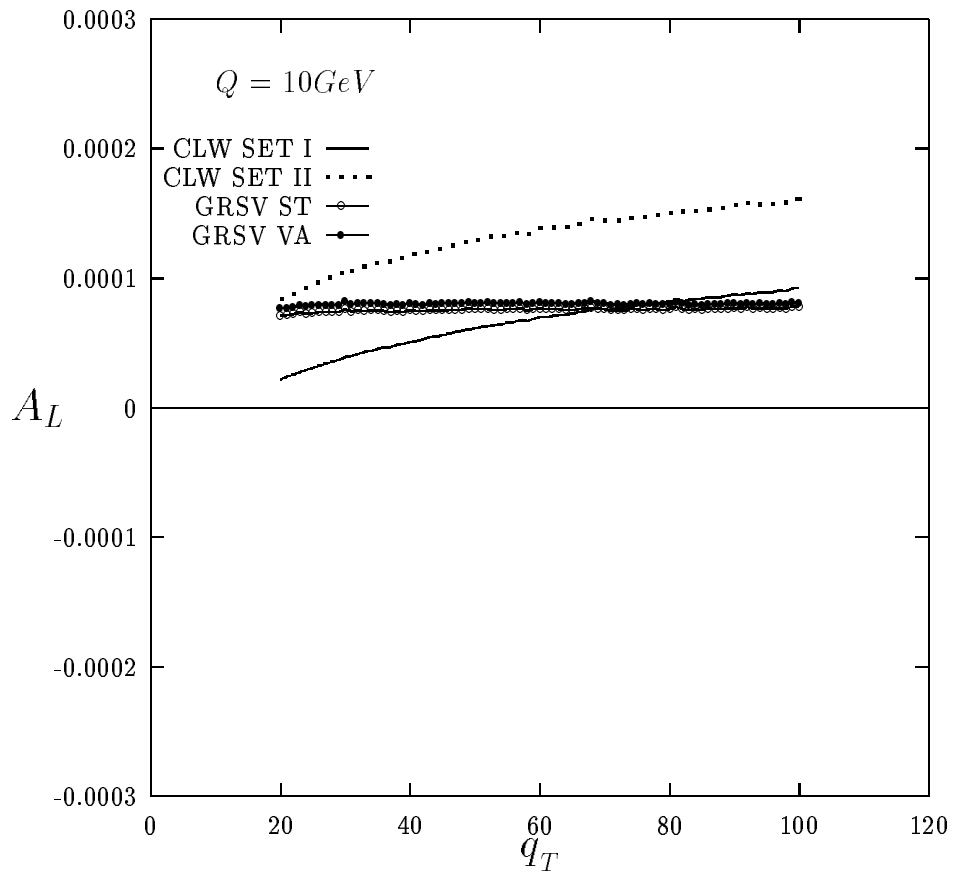


Fig.3a

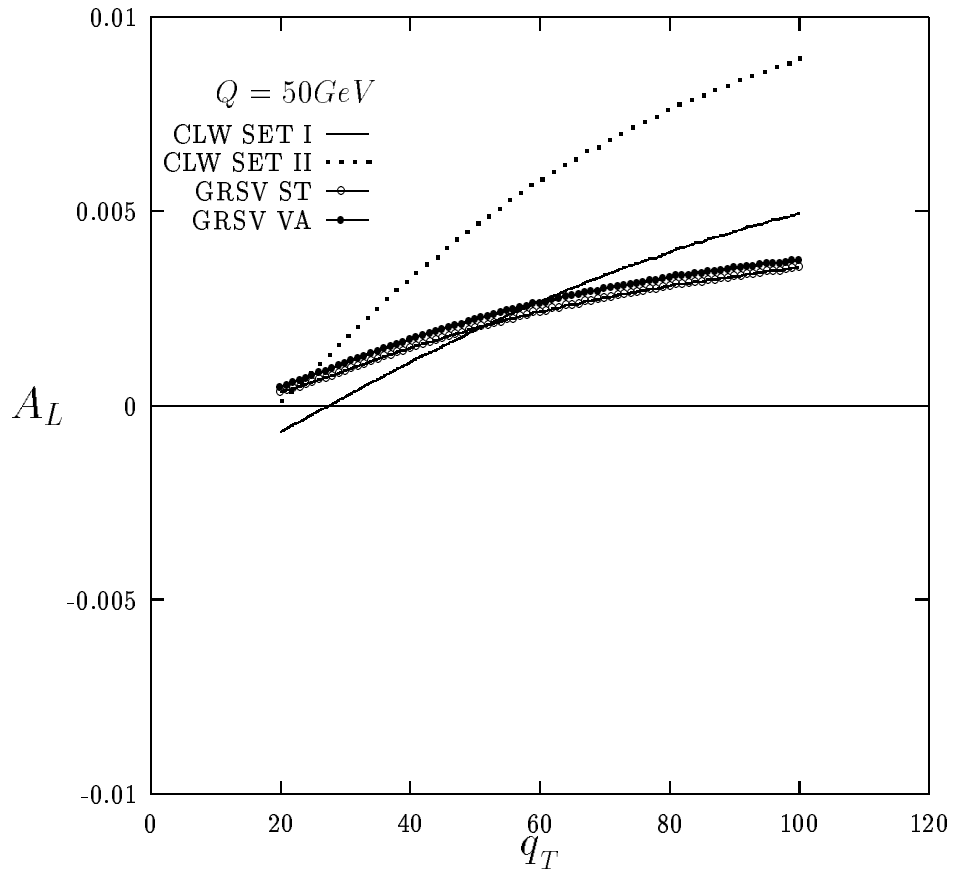


Fig.3b

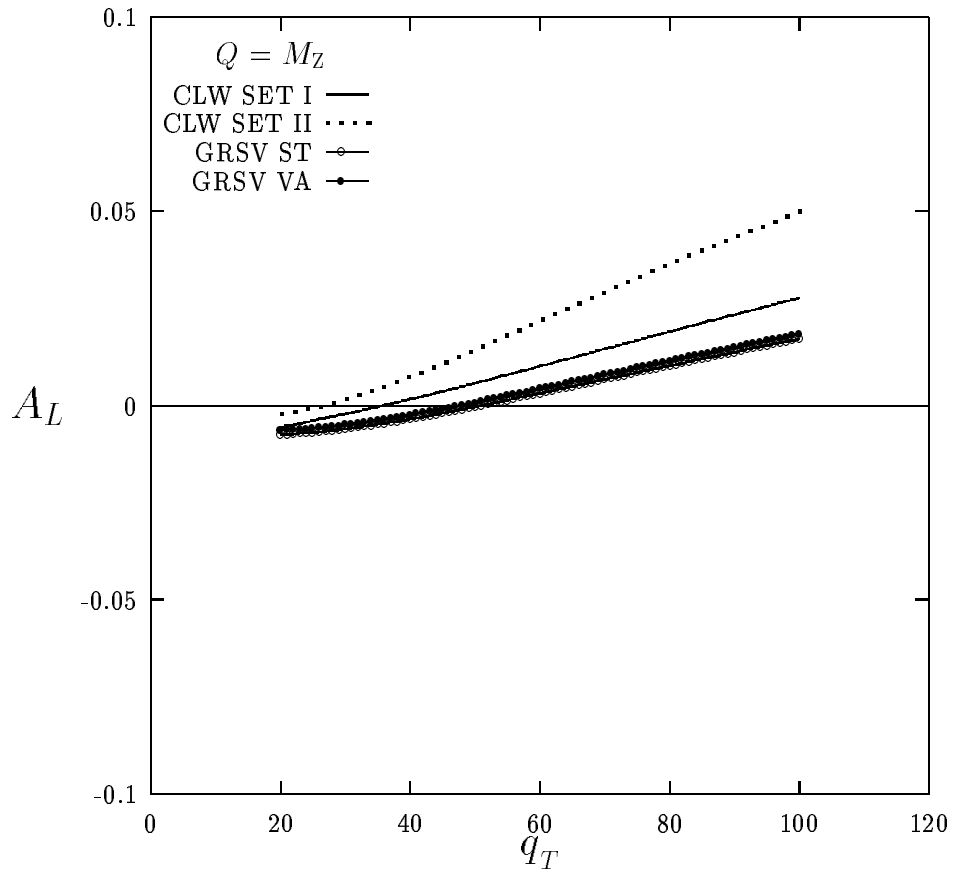


Fig. 3c

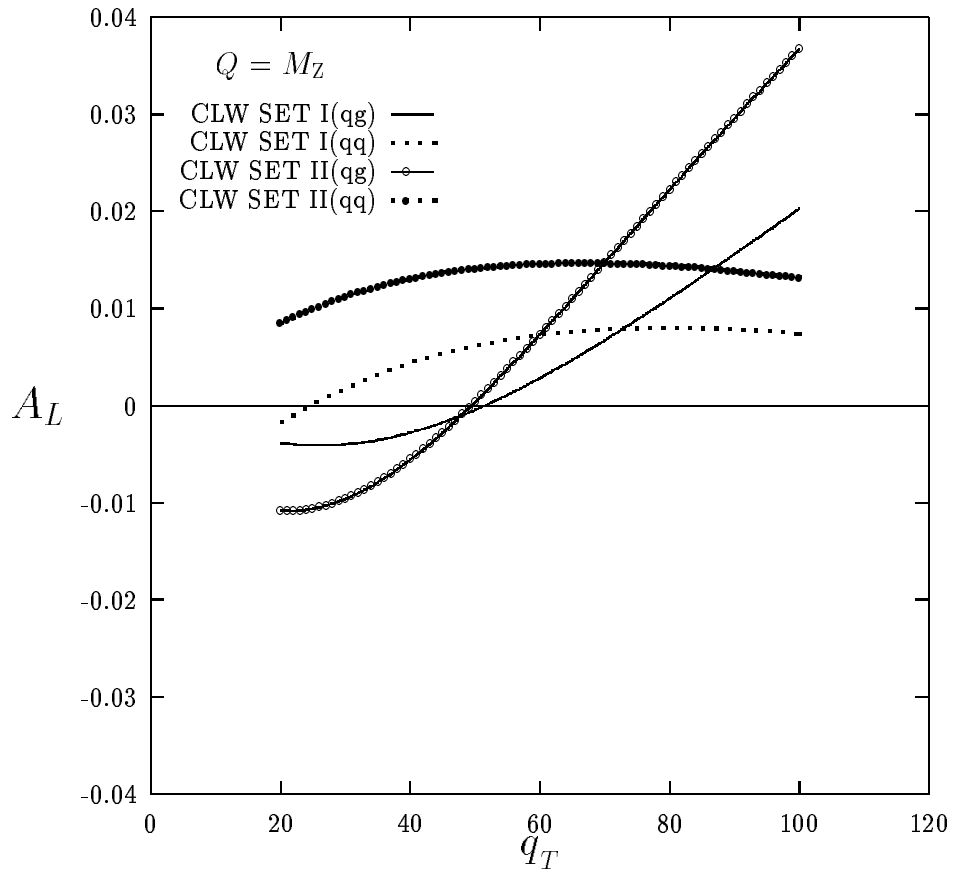


Fig.5a

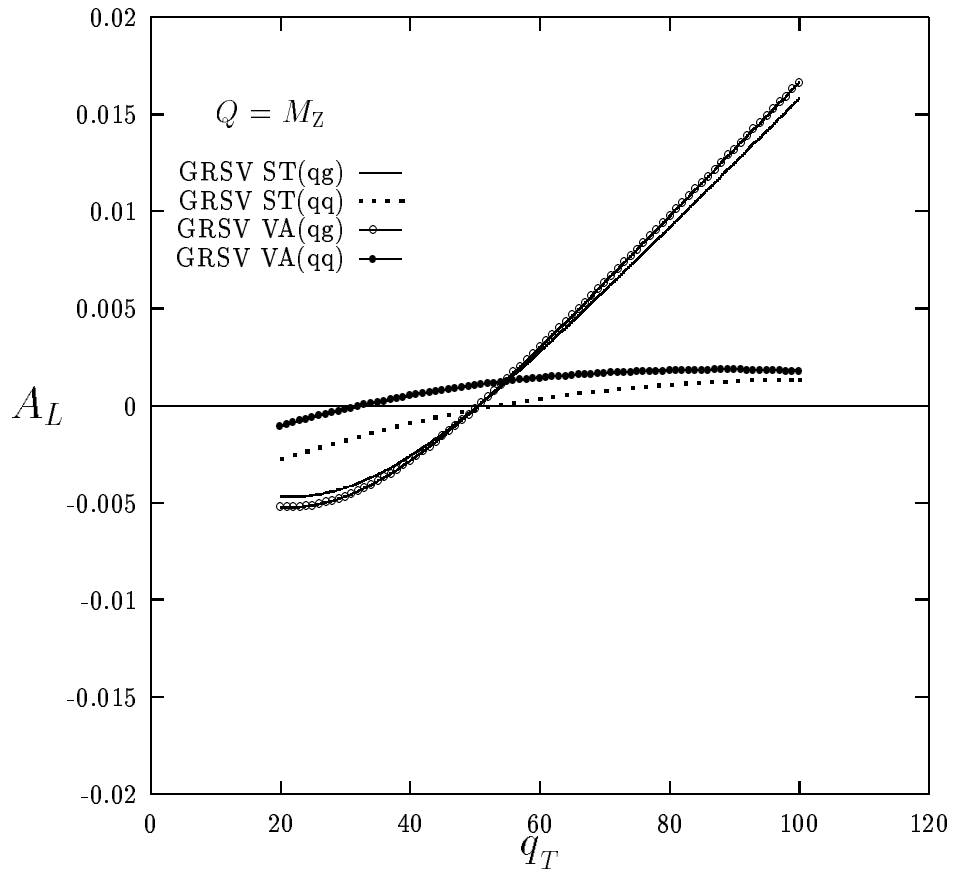


Fig.5c

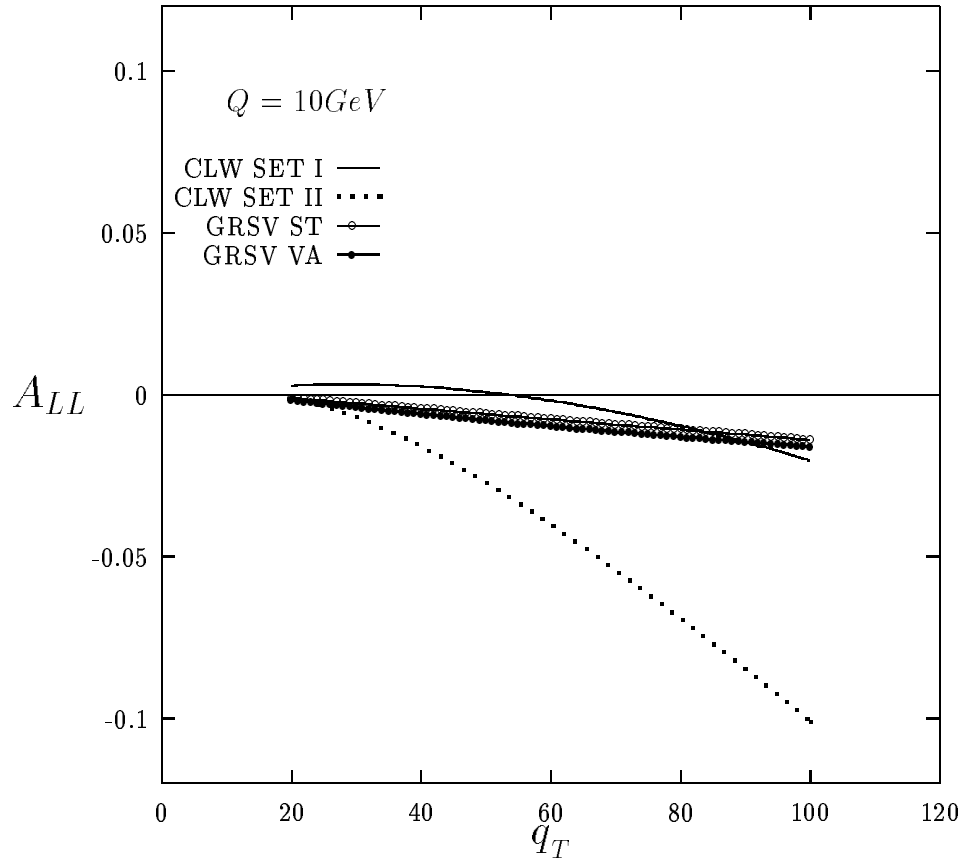


Fig.4a

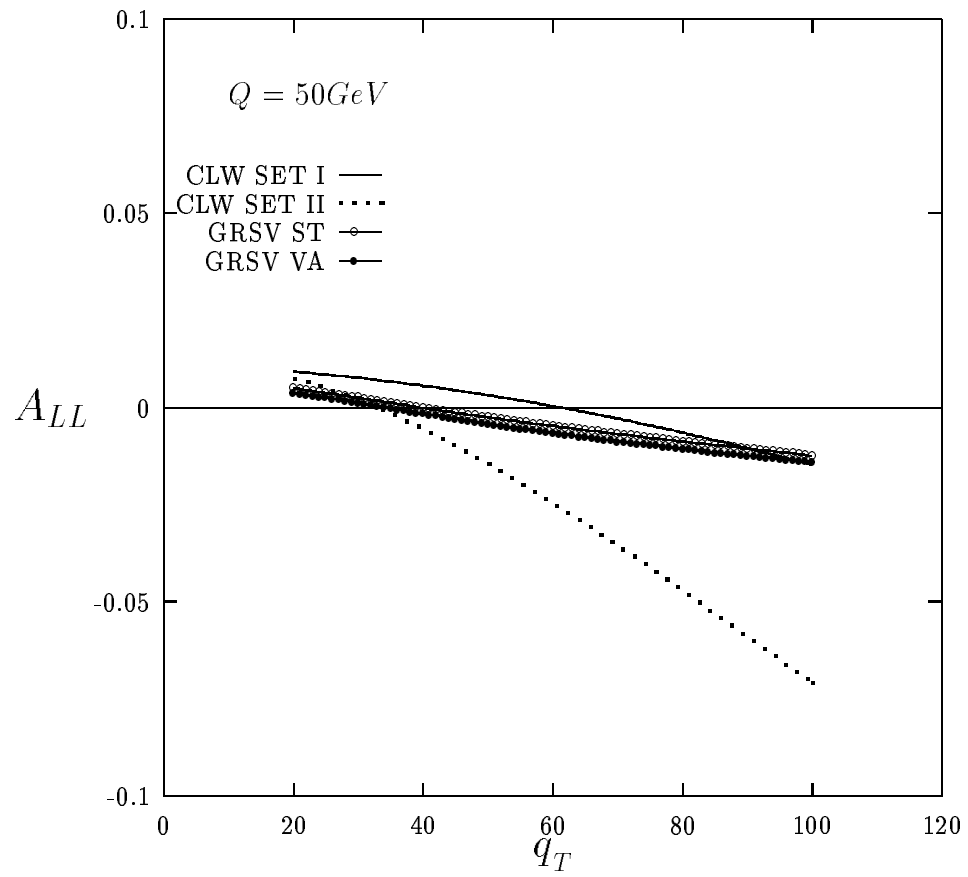


Fig.4b

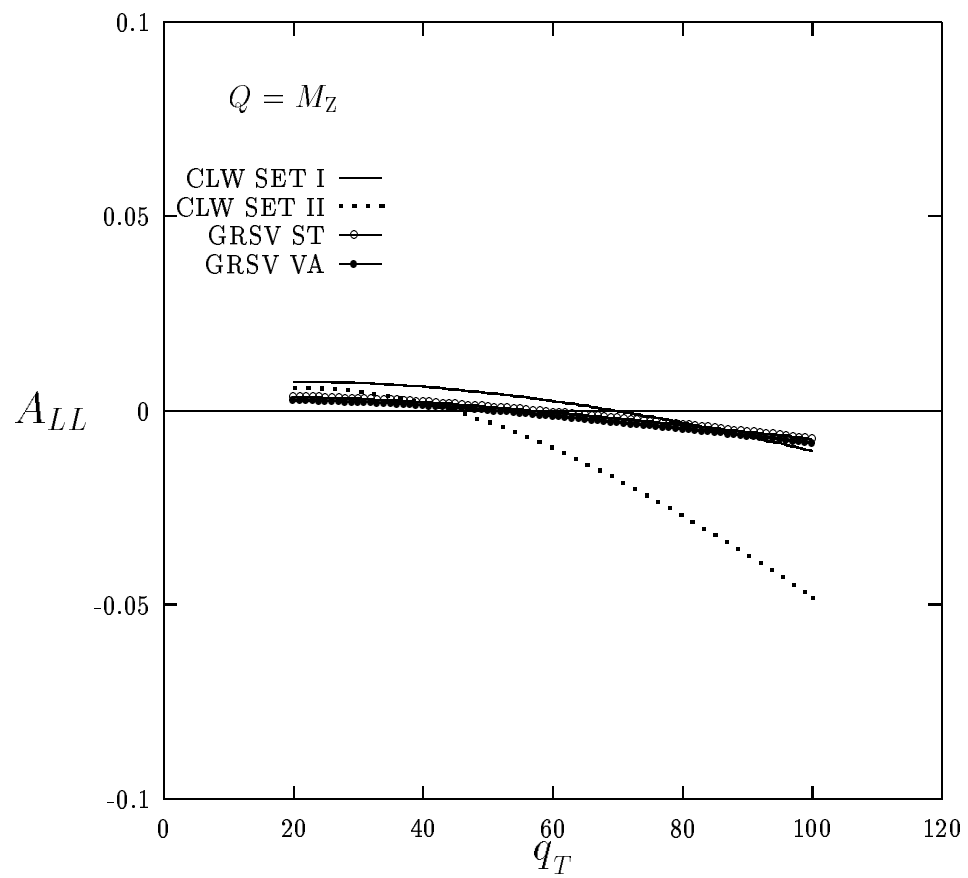


Fig.4c

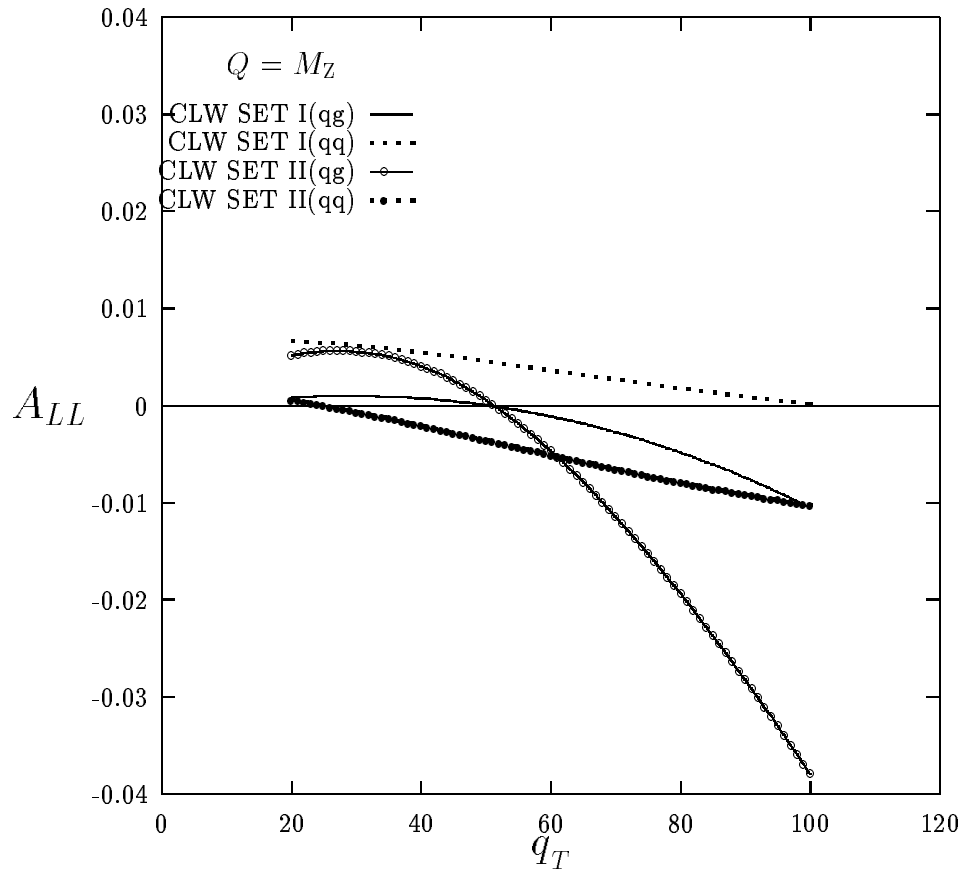


Fig.5b

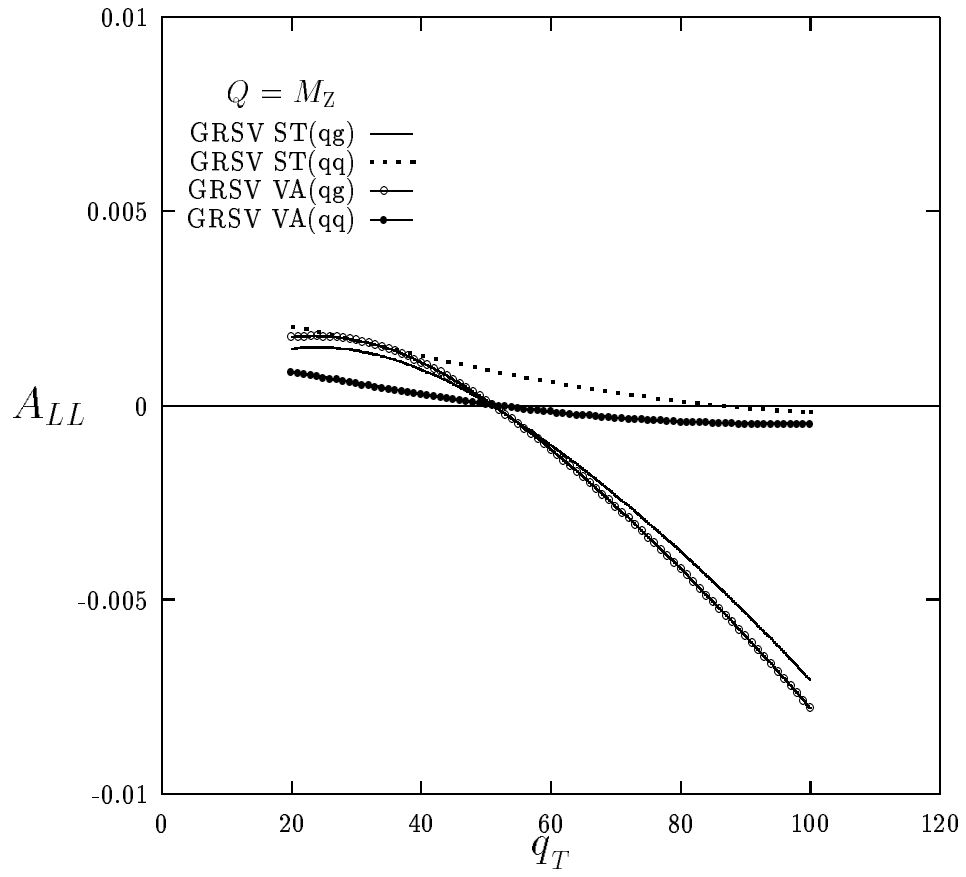
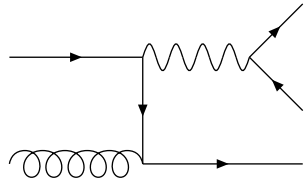
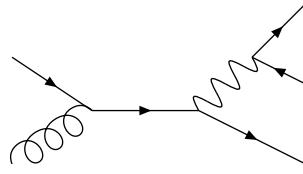


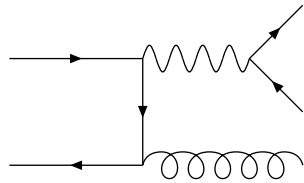
Fig.5d



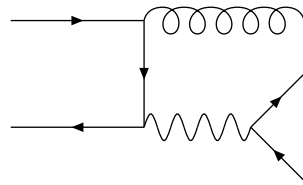
(a)



(b)



(c)



(d)

Fig. 1

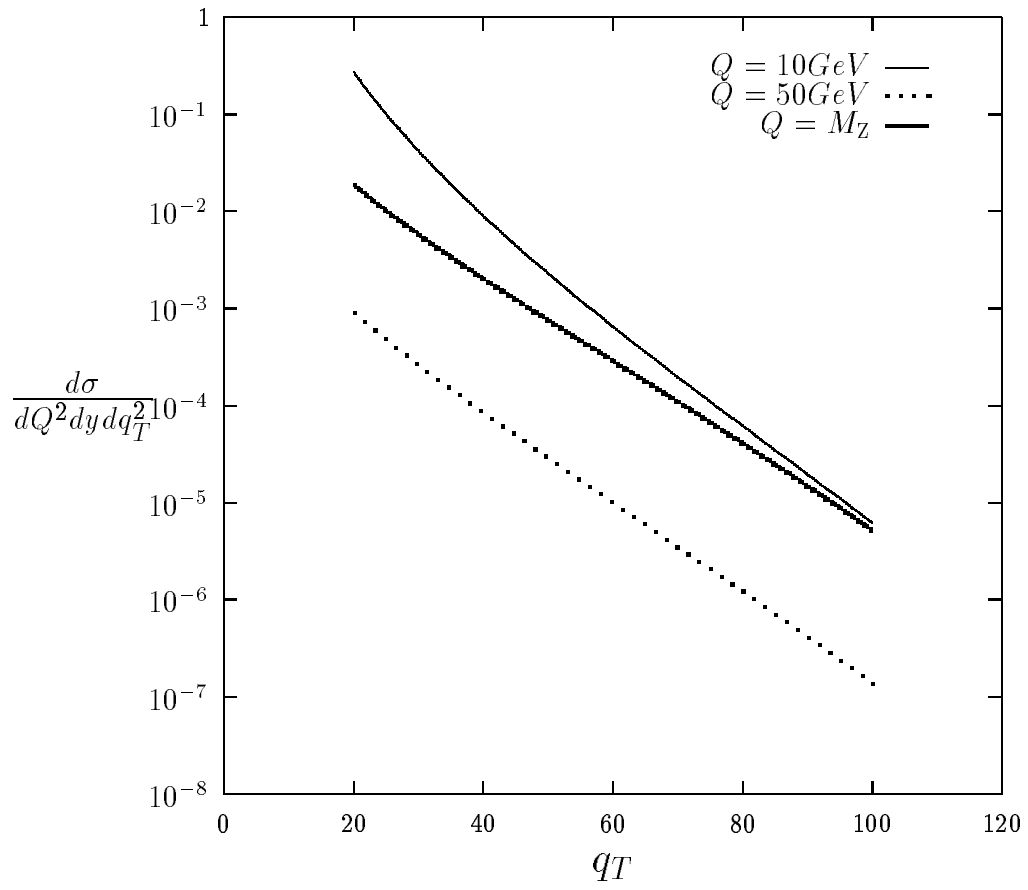


Fig. 2